Improved Current Tracking Performance of PMSM at Low Switching Frequency with Double-updating Scheme and Perfect Tracking Control

Tong Lu[1], Osamu Shimizu[2] and Hiroshi Fujimoto[3]

Abstract— **The number of poles and speed of permanent magnet synchronous motors (PMSMs) for electric vehicles (EVs) are increasing along with the development of higher power density PMSMs. Therefore, the switching-to-fundamental frequency ratios (SFRs) becomes lower at a regular switching frequency of the inverter. However, a low SFRs deteriorates the dynamic response of the current controller. Meanwhile, suppressing the torque ripple using harmonic injection becomes challenging. To address this issue, this study proposes a current controller with excellent tracking performance even at a low SFRs. Specifically, the dynamic response performance of the current controller is enhanced using the perfect tracking control (PTC) based on the double-update pulse width modulation (PWM) method. The proposed method is tested through numerical simulation, and an experiment is conducted using the surface-mounted permanent magnet synchronous motor (SPMSM). The results demonstrate that the proposed controller exhibits superior tracking performance compared to conventional methods.**

I. INTRODUCTION

Permanent magnet synchronous motor (PMSM) has been used as traction motor in electric vehicles (EVs) owing to their excellent characteristics, such as high efficiency, high power density, and wide speed regulation range. In addition, among the various EV drive systems, the in-wheel motor (IWM) drive system shows promising development prospects [1]. However, because the motors are directly installed in the wheels, the vibrations and noise generated can potentially damage the vehicle and reduce ride comfort [2]. Therefore, it is crucial to suppress the torque ripple of the IWMs, which is a significant source of vibration and noise [3], [4].

In designing IWMs, space limitations within the wheel often lead to the adoption of direct-drive motors, which eliminate the need for a gearbox. Several studies have been conducted on the design of direct-drive permanent-magnet synchronous in-wheel motors (DD-PMSIWMs). For instance, in [5], a DD-PMSIWM drive system for a campus patrol EV based on a practical driving cycle is presented, and a 46-pole rotor is adopted. In [6], PROTEAN developed a high-torque IWM for passenger cars, and adopted a 64-pole rotor. It is observed that increasing the number of pole pairs in the direct-drive in-wheel motor (DD-IWM) is necessary to achieve a high torque. For DD-IWM current control systems, the dominant approach is realized by synthesizing voltage waveform using real time digital control technique based on PWM inverter, which was initiated in the 1980's [7]. However, a higher number of pole pairs results in a higher fundamental frequency, and the switching-to-fundamental frequency ratios (SFRs) become lower at a certain switching frequency of the PWM inverter. As a result, the number of inverter pulses during PWM drive is reduced, making it more challenging to suppress harmonics and minimize the torque ripple of IWMs by control approach. Therefore, improved performance of the current controller at low SFRs is required.

Minimizing the torque ripple through the control approach of the PMSM is widely used because it can be applied to existing motors. The most prevalent control-based method is current harmonic injection [8]. However, the performance of proportional-integral (PI) controller is limited by delay and other factors, and PI control cannot track the AC signal without a steady-state error. A resonant controller is introduced in [9] to enhance the tracking performance of the PI controller and suppress current harmonics. In [10], repetitive control is employed to compensate for harmonics and suppress torque ripple. Although promising results have been achieved, their application is limited to a specified frequency and not unsuitable for machines with variable speed, such as DD-IWM. In [11], the performance of PMSM driver system at low switching frequency is improved by FPGA-based multisampling deadbeat control. In [12], in order to suppress the torque ripple well even with speed variation, a control method based on perfect tracking control (PTC) and repetitive control is proposed. In [13], to improve the tracking performance, a control method over the full operating range based on PTC is proposed. [11]–[13] verify that the proposed methods can improve the current tracking performance. However, only the case of high SFRs is discussed, and the tracking performance of AC signal is not verified.

In this study, we propose a drive system for the surface-mounted permanent magnet synchronous motor (SPMSM)-based DD-IWM. This drive system can improve the tracking performance of high-frequency AC signal at low SFRs by improving the response between sample points. The system can also be easily applied to torque ripple reduction of DD-IWM by harmonic injection approach.

II. MODELING AND TORQUE RIPPLE ANALYSIS

A. Dynamic Model of PMSM

The mathematical model of PMSM in a rotating reference (dq) frame can be expressed as follows:

$$\begin{bmatrix} v_d \\ v_q \end{bmatrix} = R_a \begin{bmatrix} i_d \\ i_q \end{bmatrix} + \frac{d}{dt} \begin{bmatrix} \psi_d \\ \psi_q \end{bmatrix} + \omega_e \begin{bmatrix} -\psi_q \\ \psi_d \end{bmatrix} \tag{1}$$

[1]T.Lu, [2]O.Shimizu, [3]H.Fujimoto are with Graduate School of Frontier Science, The University of Tokyo, 5-1-5, Kashiwanoha, Kashiwa, Chiba, 277-8561, Japan

Corresponding author: lu.tong23@ae.k.u-tokyo.ac.jp

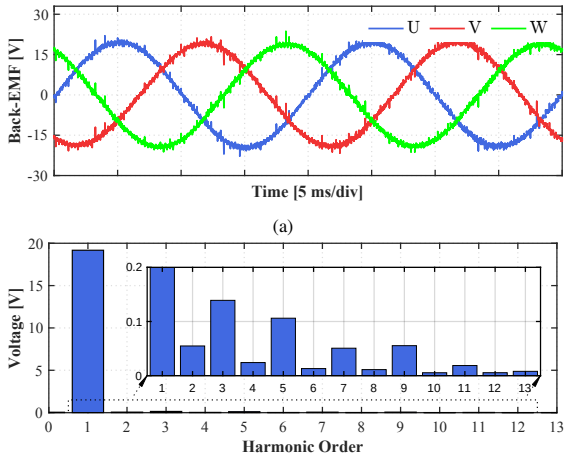

Fig. 1. Measured back-EMF waveforms and harmonic spectrum. (a) 3-phase back-EMFs at fundamental frequency f_0 = 50 Hz. (b) Harmonic spectrum.

where v_d and i_d are the d-axis stator voltage and current, respectively; v_q and i_q are the q-axis stator voltage and current, respectively; ω_e is the electrical rotor speed. Beside, ψ_d and ψ_q represent dq-axis flux linkage and can be expressed as

$$\begin{bmatrix}\psi_d\\ \psi_q\end{bmatrix}=\begin{bmatrix}L_d & 0\\ 0 & L_q\end{bmatrix}+\begin{bmatrix}\psi_a\\ 0\end{bmatrix} \tag{2}$$

where, ψ_a is the permanent magnet flux linkage.

The stator voltage equation of the PMSM without harmonic components can be obtained from (1) and (2) as

$$\begin{bmatrix}v_d\\ v_q\end{bmatrix}=\begin{bmatrix}R_a+sL_d & -\omega_e L_q\\ \omega_e L_d & R_a+sL_q\end{bmatrix}\begin{bmatrix}i_d\\ i_q\end{bmatrix}+\omega_e\begin{bmatrix}0\\ \psi_a\end{bmatrix} \tag{3}$$

where, s is the differential operator.

B. Harmonic Analysis of PMSM

The motor torque ripple is effected by the coupling of multiphysics including electric, magnetic fields, and other nonideal factors like the stator slot of the motor structure [14]. To maximize the efficiency and torque capability and reduce the torque ripple, the PMSM is desired to have a sinusoidal back-EMF and current. However, in practice, harmonics inevitably exist in the back EMF waveform. Fig. 1(a) shows the measured 3-phase back-EMF waveforms of an 8-pole PMSM at 750 r/min, and the harmonic spectrum of U-phase is shown in Fig. 1(b). As shown, the back-EMF (or flux linkage) mainly contains the 3rd, 5th, 7th, 9th order harmonics. Among them, the 3rd, 9th order harmonics is zero-sequence components, which are absent in line back-EMF of a balanced Y-connected three-phase circuit [15]. A simple proof is given below, the 3rd and 9th order harmonics of the flux linkage can be can be summarized as follows:

$$\begin{bmatrix}\psi_{\text{uh}}\\ \psi_{\text{vh}}\\ \psi_{\text{wh}}\end{bmatrix}=\sum_{\substack{k=3m\\(m=1,3)}}\psi_k\begin{bmatrix}\cos(k\omega_e t+\gamma_k)\\ \cos(k\omega_e t-2\pi m+\gamma_k)\\ \cos(k\omega_e t+2\pi m+\gamma_k)\end{bmatrix} \tag{4}$$

where ψ_{uh}, ψ_{vh}, ψ_{wh} are the harmonic components of 3-phase flux linkage, ψ_k is the harmonic amplitude of the k-order flux linkage, and γ_k is the initial phase angles of the k-order harmonic components.

Equation (5) shows the result transformed to the dq-axis. It can be observed that the 3rd and 9th order harmonic components do not affect the dq-axis.

$$\begin{bmatrix}\psi_{\text{dh}}\\ \psi_{\text{qh}}\end{bmatrix}=\boldsymbol{C}\begin{bmatrix}\psi_{\text{uh}}\\ \psi_{\text{vh}}\\ \psi_{\text{wh}}\end{bmatrix}=\begin{bmatrix}0\\ 0\end{bmatrix} \tag{5}$$

where ψ_{dh}, ψ_{qh} are the harmonic components of dq-axis flux linkage, and $\boldsymbol{C}$ is the transformation matrix from UVW coordinate to dq coordinate.

The 5th and 7th order harmonics of the flux linkage can be can be summarized as follows [15]:

$$\begin{bmatrix}\psi_{\text{uh}}\\ \psi_{\text{vh}}\\ \psi_{\text{wh}}\end{bmatrix}=\sum_{\substack{k=6n\pm1\\n=1}}\psi_k\begin{bmatrix}\cos(k\omega_e t+\gamma_k)\\ \cos(k\omega_e t-4\pi n\mp 2/3\pi+\gamma_k)\\ \cos(k\omega_e t+4\pi n\pm 2/3\pi+\gamma_k)\end{bmatrix} \tag{6}$$

The result of the transformation to the dq-axis is presented in (7). It can be observed that the 5th and 7th harmonic components would affect the dq-axis, and these harmonic components are also the reason for the torque ripple.

$$\begin{bmatrix}\psi_{\text{dh}}\\ \psi_{\text{qh}}\end{bmatrix}=\boldsymbol{C}\begin{bmatrix}\psi_{\text{uh}}\\ \psi_{\text{vh}}\\ \psi_{\text{wh}}\end{bmatrix}=\sqrt{\frac{3}{2}}\psi_k\begin{bmatrix}\cos[(k\mp1)\omega_e t+\gamma_k]\\ -\sin[(1\mp k)\omega_e t\mp\gamma_k]\end{bmatrix} \tag{7}$$

C. Torque Ripple Analysis of PMSM

The motor considered in this study is an SPMSM. For the SPMSM with inductance on the d-axis is approximately equal to the inductance on q-axis, based on (2) and (7), the electromagnetic torque is obtained as

$$\begin{aligned}T&=T_{\text{dc}}+T_{\text{ripple}}\\&=\underbrace{P_n(\psi_a i_q)}_{\text{DC term}}+\underbrace{P_n(\psi_{\text{dh}}i_q-\psi_{\text{qh}}i_d)}_{\text{Torque Ripple}}\end{aligned} \tag{8}$$

where P_n is the the number of pole pairs of PMSM.

According to (8), the torque ripple of SPMSM is obtained as follows:

$$T_{\text{ripple}}=\sqrt{\frac{3}{2}}P_n\sqrt{A^2+B^2}\sin(6\omega_e t+\delta) \tag{9}$$

$$\begin{aligned}A&=[\psi_5\cos\gamma_5+\psi_7\cos\gamma_7]i_q+[\psi_5\sin\gamma_5-\psi_7\sin\gamma_7]i_d\\B&=-[\psi_5\sin\gamma_5+\psi_7\sin\gamma_7]i_q+[\psi_5\cos\gamma_5-\psi_7\cos\gamma_7]i_d\\\delta&=\arctan(\frac{A}{B})\end{aligned}$$

Based on (9), the optimal current reference value can be designed to suppress torque ripple. For example, harmonics with the same magnitude but opposite phase of current ripple into the original reference value. However, as previously mentioned, DD-IWMs have a high fundamental electrical frequency ω_e, which results in a higher torque ripple frequency. Therefore, to minimize torque ripple through harmonic injection, a current controller with the ability to perfectly track high-frequency AC reference is particularly important.

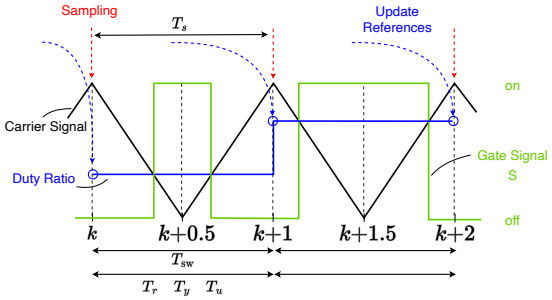

Fig. 2. Single-update PWM update and sampling scheme

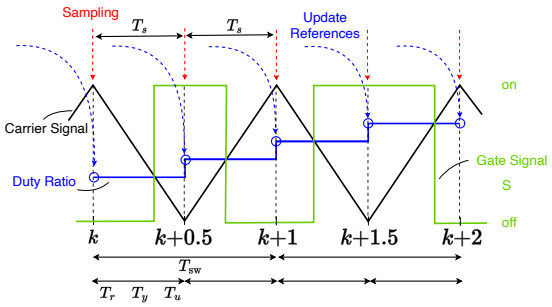

Fig. 3. Double-update PWM update and sampling scheme

III. CURRENT CONTROLLER DESIGNS

A. PWM Update and Sampling

There are two different measurement sampling and PWM updating schemes: the single-update PWM method (sampling at start or middle) as shown in Fig. 2, and the double-update PWM method as shown in Fig. 3. In the single update PWM method, the calculated modulation index is updated once in a switching period $T_{\rm sw}$. In contrast, in the double update PWM method, the modulation index is updated twice in a switching period $T_{\rm sw}$. For example, the modulation index is updated one more time at $k+0.5$ step between k step and $k+1$ step. With a carrier frequency that is half that of the conventional method, it is possible to obtain the same sampling frequency at half the switching frequency of the conventional method by 2 times oversampling. In other words, the same PWM control performance can be obtained with half the switching frequency of the conventional method by 2 times oversampling and double PWM update method. Furthermore, by updating modulation index at $k+0.5$ step, the ON time can be appropriately increased or decreased to improve the response between the original sampling points, thus better current control performance can be expected. Therefore, the double-update PWM method is chosen for the PWM update in this study, and the sampling period is denoted by T_s, the control period, sampling period of the output value, and reference values are T_u, T_y, T_r, respectively. In this study, the relationship between them is $T_s = T_r = T_y = T_u = T_{\rm sw}/2$.

B. Exact Discrete Hold-Equivalent Model

Based on the stator voltage equation of the PMSM (3), the continuous-time state-space equation without coupling terms is obtained as follows:

$$\begin{aligned}\dot{\boldsymbol{x}}(t) &= \boldsymbol{A}_c\boldsymbol{x}(t) + \boldsymbol{B}_c\boldsymbol{u}(t)\\ \boldsymbol{y}(t) &= \boldsymbol{C}_c\boldsymbol{x}(t)\end{aligned} \tag{10}$$

where the system matrices are

$$\begin{aligned}&\boldsymbol{A}_c = \begin{bmatrix}-R_a/L_d & 0\\ 0 & -R_a/L_q\end{bmatrix},\quad \boldsymbol{B}_c = \begin{bmatrix}1/L_d & 0\\ 0 & 1/L_q\end{bmatrix},\quad \boldsymbol{C}_c = \boldsymbol{I}_2\\ &\boldsymbol{x}(t) = \begin{bmatrix}i_d(t) & i_q(t)\end{bmatrix}^{\rm T},\quad \boldsymbol{u}(t) = \begin{bmatrix}v_d(t) & v_q(t)\end{bmatrix}^{\rm T}\end{aligned} \tag{11}$$

In general, the discrete-time model of system is obtained using the zero-order hold (ZOH) [16]. The ZOH method assumes that an inverter can output an arbitrary voltage. However, in the case of the precise control of instantaneous values, this method is unsuitable because the inverter output can take only 0 or $\pm V_{\rm dc}$. Therefore, system is modeled as a pulse-width modulation (PWM) hold sampled-data model [17] in this study, which can evaluate the instantaneous voltage precisely by considering the pulse width as the control input. Based on (10) the PWM hold sampled-data model can be derived as follows:

$$\begin{aligned}\boldsymbol{x}[k+1] &= \boldsymbol{A}_s\boldsymbol{x}[k] + \boldsymbol{B}_s\Delta\boldsymbol{T}[k]\\ \boldsymbol{y}[k] &= \boldsymbol{C}_s\boldsymbol{x}[k]\end{aligned} \tag{12}$$

where $\boldsymbol{A}_s = e^{\boldsymbol{A}_c T_u}$, $\boldsymbol{B}_s = e^{\boldsymbol{A}_c T_u/2}\boldsymbol{B}_c V_{dc}$, $\boldsymbol{C}_s = \boldsymbol{C}_c$. $V_{\rm dc}$ is the dc-bus voltage of three-phase inverter. $\Delta\boldsymbol{T} = [\Delta T_d \quad \Delta T_q]^{\rm T}$ are the ON time of d-axis and q-axis, and if $\Delta\boldsymbol{T} < \boldsymbol{0}$, the output voltage will be $-V_{\rm dc}$.

C. Feedforward Controller Design

To achieve superior current tracking, a feedforward controller is designed. Utilizing the future desired output in order to improve the dynamic response of the system. In this study, a oversampling feedforward controller is designed based on the method described in [18]. This method provides the response of the system to perfect tracking reference value, as long as all the initial conditions are zero, and called perfect tracking controller (PTC). The feedforward controller is a stable inverse system of the plant because the reference is the state variable $\boldsymbol{x}_d[k+1]$. Based on the strict model (12), the feedforward controller can be designed in (13). The control input is the ON time, updated every $T_{\rm sw}/2$.

$$\boldsymbol{u}_0[k] = \boldsymbol{B}_s^{-1}\left[\boldsymbol{I} - z^{-1}\boldsymbol{A}_s\right]\boldsymbol{x}_d[k+1] \tag{13}$$

Using the feedforward controller (13) and the nominal model (12), the nominal output of the system is obtained as in (14), will be used as the input to the feedback controller.

$$\boldsymbol{y}_0[k] = z^{-1}\boldsymbol{C}_s\boldsymbol{x}_d[k+1] \tag{14}$$

PTC is used to realize the pole-zero cancellation, it is proved to have a fast dynamic performance because the poles and the zeros can be placed in the desired positions precisely. If no disturbance is present, the overall transfer function from $x_d[k]$ to $y[k]$ is unity. In order to eliminate the effect of

TABLE I. PARAMETERS OF PMSM SYSTEM

Parameters	Description	Value
R_a	Winding resistance	2.1293 Ω
L_d	d-axis inductance	7.0013 mH
L_q	q-axis inductance	7.0013 mH
ψ_a	Permanent magnet flux	0.078 Wb
P_n	Number of pole pairs	4
K_t	Torque constant	0.54 Nm/A(rms)

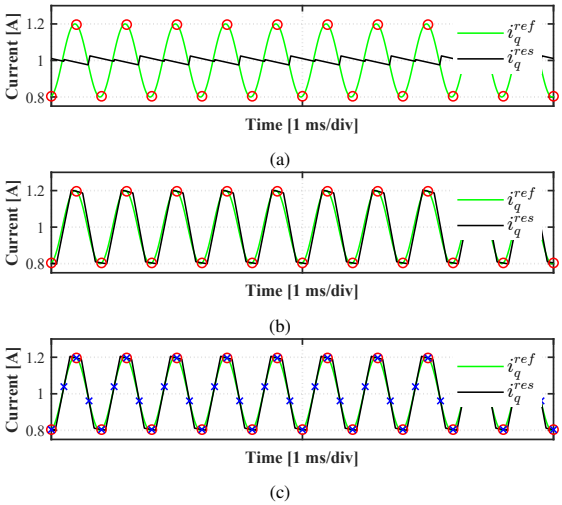

Fig. 4. Simulation results of q-axis current responses with 6-order harmonic injection under fundamental frequency f_0 = 833 Hz. (a) Conv. PI. (b) Conv. PTC. (c) Prop. Method

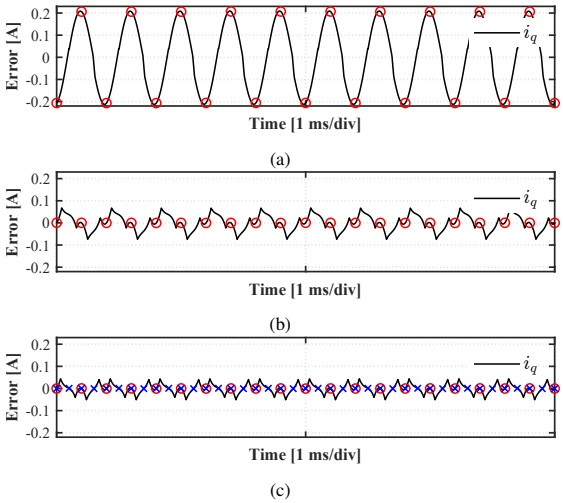

Fig. 5. Simulation results of q-axis current tracking error with 6-order harmonic injection under fundamental frequency f_0 = 833 Hz. (a) Conv. PI. (b) Conv. PTC. (c) Prop. Method

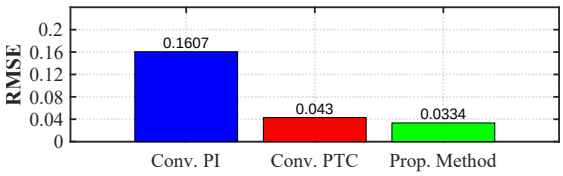

Fig. 6. Simulation result of RMSE for current tracking error

coupling terms, decoupling is achieved through feedforward compensation. The decoupling controller as follows [19]:

$$u_d^{\text{dcp}} = -\omega_e L_q i_q^{\text{res}} \tag{15}$$

$$u_q^{\text{dcp}} = \omega_e L_d i_d^{\text{res}} + \omega_e \psi_a \tag{16}$$

where i_d^{res} and i_q^{res} are the response values of the dq-axis currents, respectively.

D. Feedback Controller Design

The feedback controller is designed to ensure system robustness. Suppress the error between outputs $\boldsymbol{y}[k]$ and $\boldsymbol{y}_0[k]$ in the presence of modeling errors or disturbances. However, if none present, only the feedforward works. The major function of feedback controller is to regulate disturbance inputs or plant variations. The feedback controller is designed based on discrete PI control as follows:

$$C_{\text{fb}}[z] = \frac{(K_P + 0.5K_I T_u)z + (0.5K_I T_u - K_P)}{z - 1} \tag{17}$$

where $K_P = L_{\text{dq}}\omega_{\text{bw}}$ and $K_I = R_a\omega_{\text{bw}}$ are the controller gains and ω_{bw} is the designed closed-loop bandwidth.

IV. SIMULATION EVALUATION

The simulation model is built using MATLAB/Simulink to verify the effectiveness of the proposed method. Three control methods are compared in the simulation, conventional PI (Conv. PI), conventional PTC (Conv. PTC), and proposed method (Prop. Method), respectively. The PMSM parameters are given in Table I, and the control bandwidth of the feedback controller is ω_{bw} = 1 kHz. For Prop. Method the switching period is T_{sw} = 100 μs, and $T_u = T_y = T_r = T_{\text{sw}}/2$ = 50 μs. To evaluate the performance of the current controller at the nyquist frequency, the current reference frequency is set to 5 kHz, half the carrier frequency 10 kHz. The fundamental frequency of the motor will then be 833 Hz. This means that the SFRs will be nearly equal 12. The simulation results of the q-axis current responses are shown in Fig. 4. The simulation results of the q-axis current tracking error are shown in Fig. 5. The red circle represent the original sampling point, the blue crosses represent sampling point after oversampling. The DC component of the reference current on the q-axis is set to 1 A, and a 6-order harmonic current signal is generated based on (9), with an amplitude of 0.2 A. As shown in Fig. 4(a), It can be seen that Conv. PI control cannot track the reference. As shown in Fig. 4(b), It can be seen that the Conv. PTC has improved reference tracking on the sample points. From the tracking error results Fig. 5(b) and Fig. 5(c), it can be seen that the prop. method improves tracking performance not only on the sample points but also between the original sample points. Furthermore, the root-mean-square error (RMSE) result Fig. 6 show that prop. method is 79.22% better than Conv. PI, and 22.33% better than Conv. PTC.

V. EXPERIMENTAL VALIDATION

A. Experiment Setup

The proposed method and comparative methods are experimentally tested on a 400 W SPMSM platform, as shown

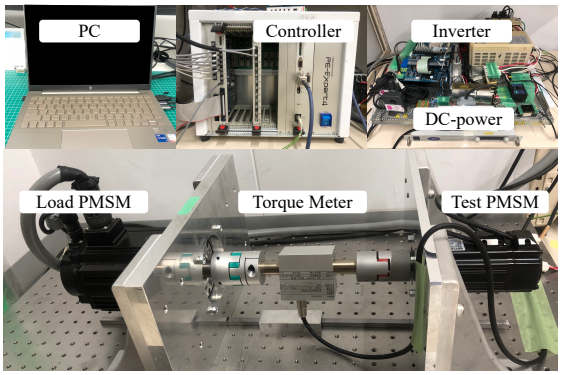

Fig. 7. Test motor and control system

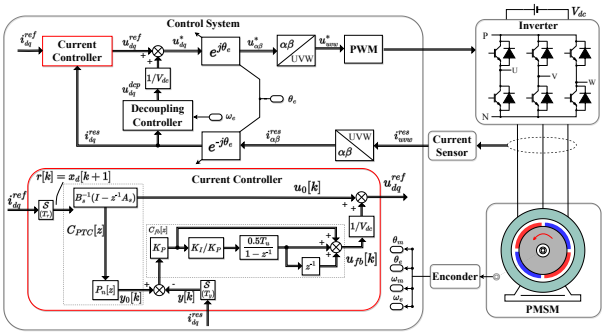

Fig. 8. Block diagram of FOC-based PMSM drive system

in Fig. 7. The control algorithm is implemented using a TMS320C6657 based digital signal processor (DSP) control board. The block diagram of the control system is shown in Fig. 8. In order to simulate low SFRs, the switching frequency of the inverter is intentionally lowered to 1 kHz. Dead time is set to 5 μs, current sampling frequency is set to 2 kHz, bandwidth of the feedback controller is set to 200 Hz, and DC voltage source is set to 200 V. The system parameters of the SPMSM are given in Table I.

B. Performance Analysis of Proposed method

Three control methods are the same as in the simulation section. Conv. PI and Conv. PTC are use the single-update PWM method, and the current sampling frequency is set to be the same as the switching frequency of the inverter, i.e., 2 kHz, and the closed-loop bandwidth is set to 200 Hz. Prop. PTC uses the double-update PWM method, the closed-loop bandwidth is set to 200 Hz. And the switching frequency of the inverter is set to 1 kHz, which is half of the current sampling frequency. By using 2 times oversampling, the current sampling frequency is 2 kHz.

To reproduce the SFRs in the simulation, the inverter switching frequency of 1 kHz and the motor fundamental frequency of 80 Hz, i.e., SFRs of Nearly Equal 12. The results of the q-axis current responses with 6-order harmonic injection at 1200 r/min are shown in Fig. 9. As shown in Fig. 9(a), the Conv. PI cannot track the AC component well. As shown in Fig. 9(b), It can be seen that the tracking performance on the sample points is improved by Conv. PTC. The results of tracking error are shown in Fig. 10. As

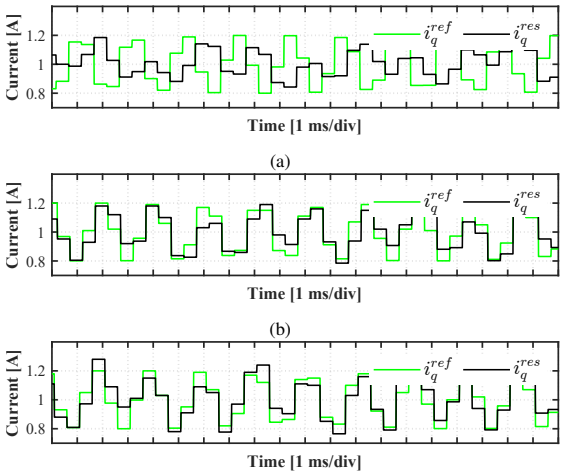

Fig. 9. Experiment results of q-axis current responses with 6-order harmonic injection under fundamental frequency f_0 = 80 Hz. (a) Conv. PI. (b) Conv. PTC. (c) Prop. Method

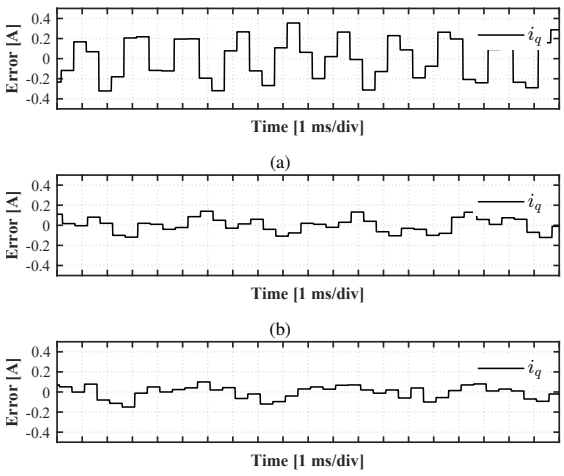

Fig. 10. Experiment results of q-axis current tracking error with 6-order harmonic injection under fundamental frequency f_0 = 80 Hz. (a) Conv. PI. (b) Conv. PTC. (c) Prop. Method

shown in Fig. 10(b) and Fig. 10(c), tracking performance between sample points has also been improved by prop. method, which further improves the tracking performance. Furthermore, the RMSE result in Fig. 11 shows that the prop. method achieves 71.44% better performance than Conv. PI, and 30.97% better performance than Conv. PTC. The current tracking performance in the range of reference frequency outside the closed-loop band is shown in Table II, which indicates that the proposed method has better tracking performance for high-frequency current than the Conv. PTC, even at low switching frequency. The gate signals of the conventional methods and the proposed method are shown in Fig. 12(a) and Fig. 12(b), respectively. From Fig. 12, it can be observed that the proposed method has half the switching frequency of the conventional methods, thus the energy loss is also lower than that of the conventional methods.

TABLE II. RMSE FOR CURRENT TRACKING AT DIFFERENT FUNDAMENTAL FREQUENCY

Fundamental frequency [Hz]	50	60	70	80
Reference frequency [Hz]	300	360	420	480
Conv. Method Ⅱ (f_{sw} = 2 kHz)	0.1077	0.0867	0.0828	0.0833
Prop. Method (f_{sw} = **1** kHz)	**0.0815**	**0.0647**	**0.0601**	**0.0575**
Improvement rate	**24.33**%	**25.37**%	**27.42**%	**30.97**%

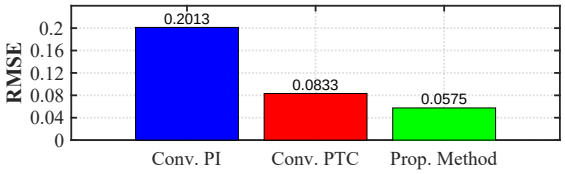

Fig. 11. Experiment result of RMSE for current tracking error

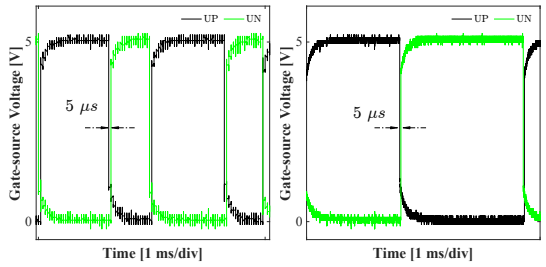

Fig. 12. Experiment results of Gate signal of U-phase with dead time T_d = 5 μs (a) conventional methods with switching frequency f_{sw} = 2 kHz. (b) proposed method with switching frequency f_{sw} = 1 kHz.

VI. CONCLUSIONS

This study proposed a current controller with high tracking performance, even at a low switching frequency. It is expected that combining the proposed method with the approach of suppressing the torque ripple through harmonic injection will be effective. At the same time, it can also be applied to machines with low SFRs, such as DD-IWMs, and can achieve a higher current control performance. In addition, because the inverter switching frequency of the proposed method is only half that of conventional methods, the energy loss of the inverter is also reduced.

As a fundamental study, comparative numerical simulations and experimental studies demonstrated the effectiveness of the proposed method using an SPMSM. In the future, we plan to apply this method to DD-IWM.

REFERENCES

[1] C. Borroni, "Making the Case for In-Wheel Motors," *SAE Automot. Eng*, vol. 8, 2021.

[2] C. Xing, Y. Zhu, and H. Wu, "Electromechanical Coupling Braking Control Strategy Considering Vertical Vibration Suppression for Vehicles Driven by In-Wheel Motors," *IEEE/ASME Transactions on Mechatronics*, vol. 27, no. 6, pp. 5701–5711, 2022.

[3] Z. Zhao, H. Taghavifar, H. Du, Y. Qin, M. Dong, and L. Gu, "In-Wheel Motor Vibration Control for Distributed-Driven Electric Vehicles: A Review," *IEEE Transactions on Transportation Electrification*, vol. 7, no. 4, pp. 2864–2880, 2021.

[4] H. S. Zhang, M. L. Yang, Y. Zhang, J. Y. Tuo, S. Luo, and J. Xu, "Analytical Calculation of Surface-Inset PM In-Wheel Motors and Reduction of Torque Ripple," *IEEE Transactions on Magnetics*, vol. 57, no. 1, pp. 1–11, 2021.

[5] X. Sun, Z. Shi, Y. Cai, G. Lei, Y. Guo, and J. Zhu, "Driving-Cycle-Oriented Design Optimization of a Permanent Magnet Hub Motor Drive System for a Four-Wheel-Drive Electric Vehicle," *IEEE Transactions on Transportation Electrification*, vol. 6, no. 3, pp. 1115–1125, 2020.

[6] C. J. Ifedi, B. C. Mecrow, S. T. M. Brockway, G. S. Boast, G. J. Atkinson, and D. Kostic-Perovic, "Fault-Tolerant In-Wheel Motor Topologies for High-Performance Electric Vehicles," *IEEE Transactions on Industry Applications*, vol. 49, no. 3, pp. 1249–1257, 2013.

[7] A. Kawamura, H. Fujimoto, and T. Yokoyama, "Survey on the Real Time Digital Feedback Control of PWM Inverter and the Extension to Multi-rate Sampling and FPGA Based Inverter Control," in *IECON 2007 - 33rd Annual Conference of the IEEE Industrial Electronics Society*, 2007, pp. 2044–2051.

[8] G. Feng, C. Lai, J. Tian, and N. C. Kar, "Multiple Reference Frame Based Torque Ripple Minimization for PMSM Drive Under Both Steady-State and Transient Conditions," *IEEE Transactions on Power Electronics*, vol. 34, no. 7, pp. 6685–6696, 2019.

[9] D. Li, Y. Iwaji, Y. Notohara, and K. Kishita, "Harmonic Current Cancellation Method for PMSM Drive System Using Resonant Controllers," in *2018 International Power Electronics Conference (IPEC-Niigata 2018 -ECCE Asia)*, 2018, pp. 1301–1307.

[10] P. Mattavelli, L. Tubiana, and M. Zigliotto, "Torque Ripple Reduction in PM Synchronous Motor Drives Using Repetitive Current Control," *IEEE Transactions on Power Electronics*, vol. 20, no. 6, pp. 1423–1431, 2005.

[11] K. Ito, R. Suzuki, K. Yoshimoto, and T. Yokoyama, "A Study of 1mhz Multisampling Deadbeat Control for Low Carrier Frequency PMSM Drive System," *IEEJ Journal of Industry Applications*, vol. 10, no. 6, pp. 669–674, 2021.

[12] T. Nakai and H. Fujimoto, "Harmonic Current Suppression Method of SPM Motor Based on Repetitive Perfect Tracking Control with Speed Variation," in *2008 34th Annual Conference of IEEE Industrial Electronics*, 2008, pp. 1210–1215.

[13] T. Miyajima, H. Fujimoto, and M. Fujitsuna, "Control Method for IPMSM Based on Perfect Tracking Control and PWM Hold Model in Overmodulation Range," in *The 2010 International Power Electronics Conference - ECCE ASIA -*, 2010, pp. 593–598.

[14] Y. Mao, S. Zuo, and J. Cao, "Effects of Rotor Position Error on Longitudinal Vibration of Electric Wheel System in In-Wheel PMSM Driven Vehicle," *IEEE/ASME Transactions on Mechatronics*, vol. 23, no. 3, pp. 1314–1325, 2018.

[15] L. Wu and Z. Lyu, "Harmonic Injection-based Torque Ripple Reduction of PMSM with Improved DC-link Voltage Utilization," *IEEE Transactions on Power Electronics*, 2023.

[16] T. Tarczewski and L. M. Grzesiak, "Constrained State Feedback Speed Control of PMSM Based on Model Predictive Approach," *IEEE Transactions on Industrial Electronics*, vol. 63, no. 6, pp. 3867–3875, 2016.

[17] K. P. Gokhale, A. Kawamura, and R. G. Hoft, "Dead Beat Microprocessor Control of PWM Inverter for Sinusoidal Output Waveform Synthesis," *IEEE Transactions on Industry Applications*, vol. IA-23, no. 5, pp. 901–910, 1987.

[18] H. Fujimoto, Y. Hori, and A. Kawamura, "Perfect Tracking Control Based on Multirate Feedforward Control with Generalized Sampling Periods," *IEEE Transactions on Industrial Electronics*, vol. 48, no. 3, pp. 636–644, 2001.

[19] O. C. Kivanc and S. B. Ozturk, "Sensorless PMSM Drive based on Stator Feedforward Voltage Estimation Improved with MRAS Multiparameter Estimation," *IEEE/ASME Transactions on Mechatronics*, vol. 23, no. 3, pp. 1326–1337, 2018.